Elsevier Editorial System(tm) for Computers and Fluids

Manuscript Draft

Manuscript Number:

Title: An Energy-Dissipative Remedy Against Carbuncle: Application to Hypersonic Flows around Blunt Bodies

Article Type: Original Research Paper

Keywords: Carbuncle, Compressible Flow, Hypersonic Flow, Residual Distribution, Finite Volume, Artificial Diffusion

Corresponding Author: Dr. Jesús Garicano Mena, Ph.D.

Corresponding Author's Institution: Universidad Politécnica de Madrid

First Author: Jesús Garicano Mena, Ph.D.

Order of Authors: Jesús Garicano Mena, Ph.D.; Andrea Lani, Ph.D.; Herman Deconinck, Professor

Abstract: The carbuncle phenomenon is a critical numerical instability preventing the accurate simulation of hypersonic flows around blunted configurations. After reviewing the known remedies to handle numerically this instability, we present and analyze in depth the only effective cure reported in literature for Residual Distribution techniques.

The shock fix, which is formulated as a locally active artificial diffusive term, depends on a single controlling parameter ε_s. Extensive testing of the fix in combination with the Residual Distribution technique allows for the determination of an optimal value for ε_s, which can be related to a local Péclet-like number.

After testing the performance of the fix in combination with the Residual Distribution technique it was originally designed for, the flexibility of the fix is demonstrated by coupling it with a cell-centered Finite Volume discretization: carbuncle instabilities are equally avoided in this case.

Finally, a number of limitations identified in the first testing phase lead to the derivation of a more physically consistent family of carbuncle fixes, whose improved capabilities are demonstrated.

An Energy-Dissipative Remedy Against Carbuncle: Application to Hypersonic Flows around Blunt Bodies

Jesús Garicano Mena[a,*], Andrea Lani[a], Herman Deconinck[a]

[a] *von Karman Institute for Fluid Dynamics, Chausse de Waterloo 72, B-1640, Rhode-Saint-Genèse, Belgium,*

Abstract

The *carbuncle* phenomenon is a critical numerical instability preventing the accurate simulation of hypersonic flows around blunted configurations. After reviewing the known remedies to handle numerically this instability, we present and analyze in depth the only effective cure reported in literature for Residual Distribution schemes.

The shock fix, which is formulated as a locally active artificial diffusive term, depends on a single controlling parameter ϵ_s. Extensive testing of the fix in combination with the Residual Distribution technique allows for the determination of an optimal value for ϵ_s, which can be related to a local Péclet-like number.

After testing the performance of the fix in combination with the Residual Distribution technique it was originally designed for, the flexibility of the fix is demonstrated by coupling it with a cell-centered Finite Volume discretization: carbuncle instabilities are equally avoided in this case.

Finally, a number of limitations identified in the first testing phase lead to the derivation of a more physically consistent family of carbuncle fixes, whose improved capabilities are demonstrated.

Keywords: Carbuncle, Compressible Flow, Hypersonic Flow, Residual Distribution, Finite Volume, Artificial Diffusion

*Corresponding author, currently at Universidad Politécnica de Madrid.
Email address: jesus.garicano.mena@vki.ac.be (Jesús Garicano Mena)

1. Introduction - the carbuncle instability and the known remedies

In the shock-capturing methods community, the numerical instability that appears recurrently when simulating high Mach number flows around blunted geometries with flux difference splitting (or Godunov type) schemes and shock surface aligned meshes is known as *carbuncle*. The name comes from the appearance of the computed shock profile, featuring a *blister* growing upstream of the normal-shock part of the bow shock (where the fluid is undergoing a supersonic to subsonic compression), as in Figure 1. The flow structure is what would result if a nail were placed in the stagnation point of the body: two oblique shock waves attached to the *nail* projecting backwards, that at some point interact with the bow shock profile of the blunt body. Since this happens when no nail is present, the post-shock conditions are unphysical and the computed flow field is entirely wrong.

Throughout the bibliography regarding this subject ([1, 2, 3, 4, 5],...), the carbuncle phenomenon is observed *mainly*[1] when using schemes with the desirable property of preserving steady contact waves -*e.g.* the *RD* N-scheme [8], and other well established *FV* schemes (*e.g.* Godunov, Roe and Osher schemes). Whether a carbuncle appears or not depends on the mesh employed; the bibliography agrees on that the presence of cells elongated across the shock profile favors the appearance of the instability [4]. Another fact observed is that the higher the Ma number is, the more likely it is to obtain a carbuncle, with $Ma = 6$ as the threshold traditionally accepted for a well-developed carbuncle. However, some weaker forms of instability (shock profile thickening) can be observed at Ma as low as 1.5 [5].

The first analysis of the carbuncle phenomenon was carried out by Quirk in [1]. There, he realized that the dimensionally-splitted *FV* Roe scheme, typically affected by carbuncle

[1] We stress the *mainly* here because [6, 7] disprove the widespread belief that dissipative schemes as Van Leer or Hänel do not present shock instabilities. It is true that they don't present protruding carbuncle as contact wave preserving schemes do, yet some [7, ...*multidimensional shock anomalies for a mesh either with a large number of cells in the shock parallel direction or a large cell* AR] can be observed.

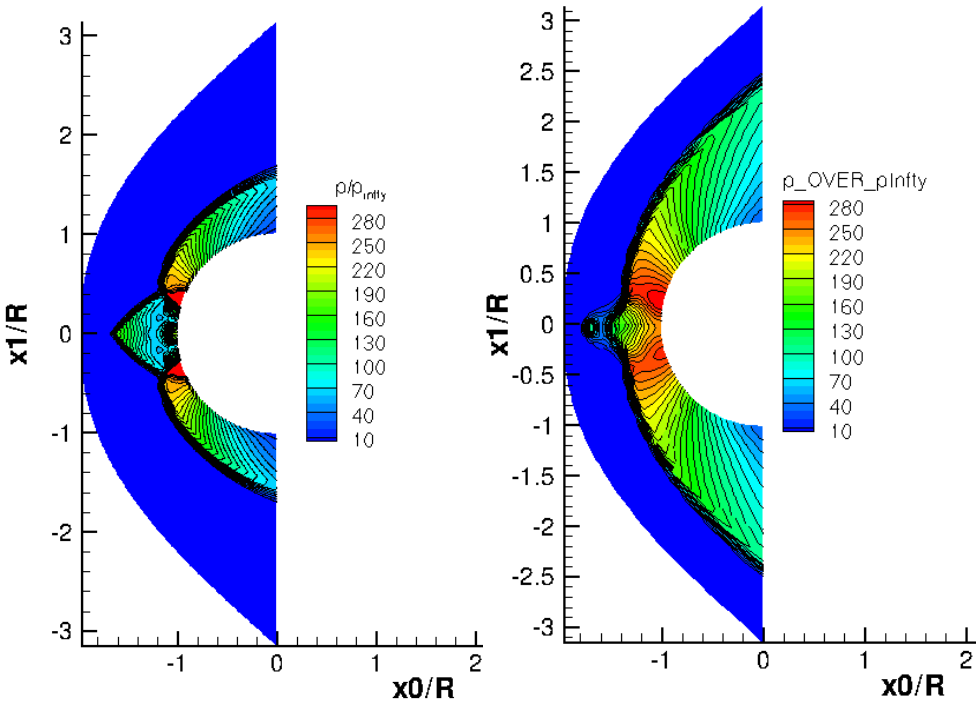

(a) *RD N* scheme. No fix applied.

(b) *FV Roe* scheme. No fix applied.

Figure 1: Carbuncle flawed solutions.

for blunt body simulations, is as well unable to preserve the shock profile flatness of a normal shock wave propagating along a straight channel on a uniform mesh but with the central grid line being a small sawtooth profile (amplitude of 1×10^{-6} over 1)[2]. This subtle modification is enough to induce sawtooth perturbations in the pressure and density profiles along the shock wave. In short, this implies that different sections of the shock profile propagate at different speeds (since the local sound speed is different). Under

[2]This configuration (and variations of it) is now known as Quirk's test. These Quirk's tests, that replicate somehow the normal region of a bow shock wave, are an important research tool regarding carbuncle phenomena, since they allow to characterize a scheme behavior face to numerical instabilities in multidimensional situations studying these simpler $1D$ problems (see for example [4] and [7]).

some conditions, these perturbations will not damp out but amplify, and the shock profile will break down. Quirk observed an equivalent behavior (confirmed theoretically in later studies [3] and [5]) in flow simulations around blunted geometries, that could be triggered even by round-off errors in any trivial manipulation of the numerical flow field.

Since Roe scheme's property of preserving steady contact waves prevents the crosswind perturbations to damp out, Quirk proposed -as a remedy- to increase locally the crosswind dissipation in the numerical solution, by flagging the cells crossed by a shock wave using a tunable pressure based detector and using there a more diffusive scheme (in his case, Einfeldt's *HLLE* [9]). This remedy solves the problem for the $1D$ shock wave propagation, and when applied to flow over blunt bodies, prevents carbuncle to appear. This is the first known *cure* for the carbuncle phenomenon.

Dissatisfied with the constrains of Quirk's carbuncle fix formulation (tunable shock detector, two different schemes involved, dimension by dimension extension of $1D$ ideas), Sanders *et al.* proposed another fix in [2], of multidimensional nature and using a single scheme (either Roe's or Godunov's), which they applied to a structured grid *FV* solver. This fix increases locally the crosswind dissipation as well, by applying an entropy fix correction [10] to the flux function computed at every cell interface. Multidimensionality comes from considering the maximum entropy correction among a given cell interface and all others that intersect it. For $2D$ structured, regular grids the corresponding stencil is H-shaped, and hence the name of H-correction. Later on, Pandolfi and D'Ambrosio reported in [4] the appearance of carbuncle in viscous computations; H-correction algorithm was able to prevent shock instabilities for Navier-Stokes computations as well, but with a tendency to over diffuse boundary layers. Thus they refined the H-correction algorithm by removing from its stencil the current interface where the flux function is to be computed. In this way, the fix is not activated when in presence of a transverse density gradient, what avoids erroneously diffusing boundary layers.

Ismail, in [11], after extensive study of many Quirk's tests, identified a correlation between spurious post-shock vorticity and the crosswind perturbations characteristic of carbuncle flawed solutions. From this observation, the author proposes techniques to control vorticity. However, he finds that acting on vorticity does not suffice to avoid carbuncle. The author suggests then to ensure that entropy is effectively produced at shock waves; he finds that if the flux functions are evaluated at a particular averaged inter-cell state (depending on a single parameter), then no carbuncle appears for a wide range of test conditions.

This article is organized as follows: next section describes the equations governing the inviscid perfect gas hypersonic flows we are interested in. Section 3 presents and discusses thoroughly the only carbuncle fix applicable to Residual Distribution (*RD*) schemes, which we term the Standard fix; its performance in the context of *RD* methods is first evaluated in subsection 3.2. The Standard fix is extended and applied for the first time together with a Finite Volume (*FV*) method in subsection 3.3. Section 4 addresses several shortcomings of the Standard fix and derives a novel Energy-Dissipative family of carbuncle fixes which solve the aforementioned limitations. Finally, section 5 summarizes our findings.

2. Governing equations

The flows of our interest are described by the Euler system of equations, which expresses the conservation of mass, momentum and energy of a fluid parcel. This system of equations writes as:

$$\begin{array}{lll} \dfrac{\partial \rho}{\partial t} & +\nabla\cdot(\rho\vec{u}) & = 0, \\ \dfrac{\partial \rho\vec{u}}{\partial t} & +\nabla\cdot\left(\rho\vec{u}\cdot\vec{u}^t + p\bar{\bar{I}}_{n_D}\right) & = 0, \\ \dfrac{\partial \rho E}{\partial t} & +\nabla\cdot(\rho H\vec{u}) & = 0. \end{array} \tag{1}$$

In equation above, ρ stands for the gas density, and $\rho\vec{u}$ and ρE are the momentum and the total energy per unit volume, respectively. Additionally, p is the pressure exerted by the

gas and H is the specific total enthalpy, which reads:

$$H = E + \frac{p}{\rho}. \tag{2}$$

The specific total energy E gathers both the specific internal energy e and the specific kinetic energy:

$$E = e + \frac{\|\vec{u}\|^2}{2}. \tag{3}$$

System of equations 1 is not closed till an equation of state and adequate initial and boundary conditions are provided.

Despite the modeling of hypersonic flows can involve complex thermodynamic models (see [12]), for our purpose of generation and cure of carbuncle instabilities the perfect ideal gas (*PG*) model is enough. Therefore, we consider the gas to be calorically and thermally perfect, hence:

$$p = R_g \rho T \text{ and } e = C_v T. \tag{4}$$

The gas constant R_g depends on the molecular weight of the gas under consideration. For air ($M_{air} = 28.84 kg/kmol$), $R_{air} = 288.29 J/K\, kg$; the specific heat capacity at constant volume C_v, which is constant for a calorically and thermally perfect gas, is given by:

$$C_v = \frac{R_g}{\gamma - 1},$$

with $\gamma = 1.4$, since air is considered a mixture of diatomic molecules.

The relation between pressure and the conserved quantities is trivial in this case:

$$p = (\gamma - 1)\left(\rho E - \frac{1}{2}\rho \|\vec{u}\|^2\right). \tag{5}$$

As for what are *adequate* initial/boundary conditions for the system of non-linear partial differential equations in Eq. 1 on the space-time domain $\Omega \times [0, T]$ is in itself a complex mathematical problem: the interested reader can refer to [13, 14].

To ease the mathematical manipulations that we will present in sections 3 and 4, the system of Eqs. 1 can be cast in compact vector form as:

$$\frac{\partial \vec{U}}{\partial t} + \nabla \cdot \bar{\bar{F}}^c = \vec{0}, \tag{6}$$

where $\vec{U}$ stands for the vector of conserved variables. For the considered *PG* model:

$$\vec{U} = \left[\rho, \quad \rho u_j, \quad \rho E\right]^t, \tag{7}$$

and tensor $\bar{\bar{F}}^c$, describing the convective flux of the conserved quantities, is (Einstein convention applies):

$$\bar{\bar{F}}^c = \vec{F}_j^c \cdot \vec{1}_j^t, \text{ for } j \in \{x_1, \ldots, x_{n_D}\}.$$

The components of the convective flux tensor $\vec{F}_j^c$ are:

$$\vec{F}_j^c = \left[\rho\, u_j, \quad \rho\, \vec{u}^t\, u_j + p\vec{1}_j, \quad \rho\, H\, u_j\right]^t, \; j \in \{x_1, \ldots, x_{n_D}\}. \tag{8}$$

The vectors employed fulfill:

$$\vec{U},\ \vec{F}_j^c \in \mathbb{R}^{n_{Eqs}} \text{ and } \left\{\vec{1}_j\right\} \text{ is the canonical basis for } \mathbb{R}^{n_D}.$$

For the *PG* model, the number of equations is given by $n_{Eqs} = n_D + 2$, where n_D is the geometric dimension of the problem.

3. A carbuncle fix based on artificial dissipation

From the discussion in section 1, there is a link between numerical perturbations along the normal-shock region of a shock wave and the carbuncle phenomenon. If what it takes to avoid the shock instability is to damp out such perturbations, so that their growth is disrupted and the carbuncle formation is prevented, then adding dissipation through an artificial diffusive term could, in principle, be as effective as any of the strategies described in section 1.

Addressing the carbuncle instability through an artificial diffusive term has several advantages: it avoids modifying the advective Jacobian eigenvalues through an entropy fix physically unrelated to carbuncle, it also saves some of the computational complexity of mixing two differently behaved schemes. On top of that, discretizing a dissipative term extends to general unstructured grids more easily than fixes based on H-stencil, tailored to structured, cell-centered meshes.

Sermeus and Deconinck worked along this line and proposed a remedy against carbuncle in the framework of *RD* schemes in [15]. They supplemented Eq. 1 with an artificial diffusive term affecting the momentum conservation equation projected along the streamlines:

$$\frac{\partial \rho u_\xi}{\partial t} \quad + \nabla \cdot \left(\rho u_\xi \vec{u}^t + p \vec{1}_{\rho\, u_\xi} \right) \quad = \frac{\partial}{\partial \eta} \left(\underbrace{\mu_s \frac{\partial u_\xi}{\partial \eta}}_{D} \right), \tag{9}$$

where $\vec{1}_\xi \in \mathbb{R}^{n_D}$ is the unit vector aligned with the local flow speed. Choosing appropriately another versor $\vec{1}_\eta$, a right handed system of reference $\left(\vec{1}_\xi, \vec{1}_\eta\right)$ can be defined, see Fig. 2.

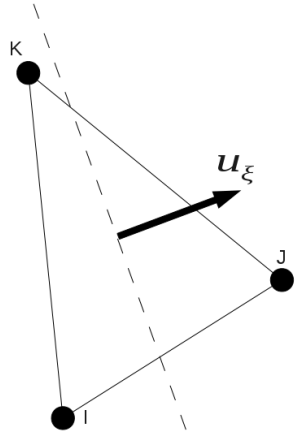

Figure 2: Local system of reference (ξ, η).

The influence of the fix in the global system of reference is obtained through the following transformation:

$$\begin{aligned} \vec{1}_{\rho\, u_\xi} &= \cos\theta\, \vec{1}_{\rho\, u} + \sin\theta\, \vec{1}_{\rho\, v}, \\ \vec{1}_{\rho\, u_\eta} &= -\sin\theta\, \vec{1}_{\rho\, u} + \cos\theta\, \vec{1}_{\rho\, v}, \end{aligned} \tag{10}$$

with θ the angle of the local streamline with the *global* x axis.

3.1. RD discretization of the carbuncle fix

In this section we address exclusively the discretization of the artificial diffusive term. For further details on the ***RD*** technique the reader is referred to AppendixA and the bibliography therein. The ***RD*** computations shown in this and the next sections have been performed with the ***RD*** solver provided by the `COOLFluiD` computational framework [16].

The fix term is discretized as an standard dissipative term, see Eq. A.13; its contribution to the l-th nodal residual is:

$$\vec{\Phi}_l^{ad} = \int_{\Omega_i} \omega_l^{\Omega_i}\, D\vec{1}_{\rho\, u_\xi}\, dV = -\mu_s \frac{n_{\eta,l}}{4\Omega_i} \sum_{k=1}^{3} n_{\eta,k}\, u_{\xi,k} \vec{1}_{\rho\, u_\xi} = -\mu_s \frac{n_{\eta,l}}{2} \left.\frac{\partial u_\xi}{\partial \eta}\right|^h . \tag{11}$$

Unit vector $\vec{1}_{\rho\, u_\xi}$ stresses out that the fix affects exclusively the momentum conservation equation along streamlines. Please notice that, despite $\vec{1}_\xi$ and $\vec{1}_{\rho\, u_\xi}$ both relate to the local streamwise direction, $\vec{1}_\xi \in \mathbb{R}^{n_D}$ and $\vec{1}_{\rho\, u_\xi} \in \mathbb{R}^{n_{Eqs}}$.

All quantities in Eq. 11 are known in the global system of reference:

$$\begin{aligned} n_{\eta,k} &= -\sin\theta\, n_{x,k} + \cos\theta\, n_{y,k}, \\ u_{\xi,k} &= \cos\theta\, u_k + \sin\theta\, v_k. \end{aligned} \tag{12}$$

Sermeus and Deconinck applied the artificial dissipation only in those cells where the flow undergoes a supersonic to subsonic compression. In order to identify them, let I be the set of vertices of element Ω_i, and call I_{super} and I_{sub} the subsets of vertices where Ma

number is supersonic and subsonic respectively. Cell Ω_i *contains* part of the supersonic-to-subsonic compression region if the following conditions hold:

$$\Omega_i \mid I = I_{super} \cup I_{sub},\ I_{super},\ I_{sub} \neq \emptyset, \qquad \nabla Ma|^h \cdot \vec{1}_\xi < 0. \tag{13}$$

Alternatively, in this contribution we prefer to apply the carbuncle fix uniformly over the whole numerical shock region. A means to locate the shock is therefore needed: we use the detector function described in [17], adapted to our ***RD*** discretization technique:

$$\sigma^{\Omega_i} = \cos^2\left(\frac{\pi\, Z}{2}\right), \tag{14}$$

where

$$Z = min(1, max(0, z)) \text{ and } z = \frac{\phi_{max} - \phi}{\phi_{max} - \phi_{min}},$$

with ϕ defined as

$$\phi = \frac{\max\limits_{j \in \Omega_i} v_j}{\min\limits_{j \in \Omega_i} v_j}, \text{ with } v = p,\ T \text{ or } \rho,$$

and one takes typically $\phi_{max} = 3$ and $\phi_{min} = 2$.

The fix depends on the parameter μ_s, estimated originally [15] as:

$$\mu_s = \epsilon_s\, h\, \lambda_{max}\ \left[L^2\, T^{-1}\right], \tag{15}$$

where h characterizes the size of the cell, λ_{max} is the maximum eigenvalue in absolute terms and ϵ_s is a tunable parameter. Here, and for a closer resemblance to a physical dissipative term, we have preferred to redefine μ_s [18] as:

$$\mu_s = \epsilon_s\, h\, \rho_{avg}\, \lambda_{max}\ \left[M\, L^{-1}\, T^{-1}\right]. \tag{16}$$

Through this new definition it is possible to relate the fix single controlling parameter ϵ_s with a cell Péclet number:

$$Pe^{\Omega_i} = \frac{\frac{\rho_{avg}\, \lambda_{max}^2}{h}}{\frac{\mu_s\, \lambda_{max}}{h^2}} = \frac{1}{\epsilon_s}. \tag{17}$$

3.2. Results: RD and Carbuncle Fix

We present here a sensitivity analysis of the fix with respect to its only controlling parameter, ϵ_s. As test case, the hypersonic inviscid flow field over an infinite-span cylinder of $50.8\,mm$ in diameter has been simulated. The free stream conditions, chosen to match those in [19], are given in Table 1. Several simulations have been performed on a 31×401 nodes triangulated mesh (31 equispaced nodes over the cylinder wall and 401 along the radial direction, see Fig. 3a; no attempt to align the grid with the shock surface has been made), each time with a different value of ϵ_s.

Table 1: Free stream conditions.

Ma_∞	$D[m\,m]$	$\rho_\infty\,[kg/m^3]$	$U_\infty\,[m/s]$	$T_\infty\,[K]$	$p_\infty\,[Pa]$
15	50.8	0.00922	4688.15	241	640.53

The steady solution to the semi-discretized System of Equations A.6 is obtained through implicit backward Euler integration; the resulting intermediate linear problems are solved using Krylov subspace methods [20] in combination with parallel preconditioners such as the Additive Swartz Method, as implemented in the `PETSc` library [21].

For the discretization of the advective term we have chosen the matrix N scheme, Eq. A.8. The N scheme, and its variants, is possibly the most used *RD* scheme for the simulation of shocked flow fields [8, 22, 23, 24]. The N scheme, being a multi-dimensional generalization of the classical *FV* Roe scheme [25], is prone to generate carbuncles, as shown in Figure 1a.

The results of the parametric sensitivity study are summarized in Table 2 and in Fig. 4. We observe in Fig. 4a, that for $\epsilon_s = 0.05$ the protruding carbuncle shown in Fig. 1a has been greatly reduced, though the solution is clearly not yet correct. Increasing ϵ_s to 0.1 yields a solution with no trace of carbuncle, Fig. 4b. Increasing further ϵ_s to 0.5 and larger

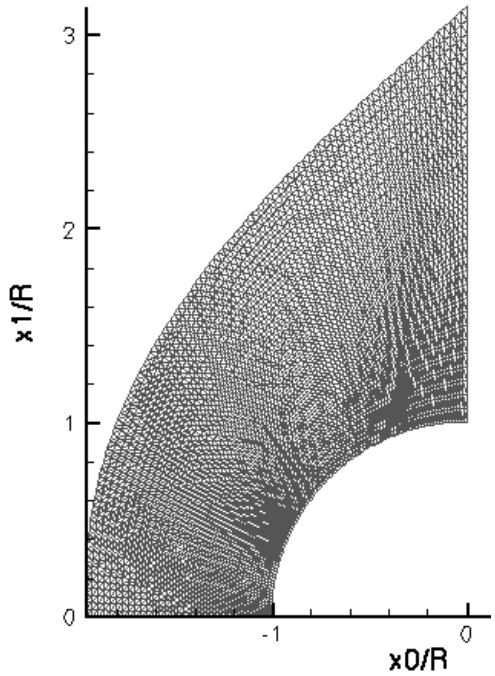

(a) Triangular mesh, 31×401 nodes($\sim 1.2 \times 10^4$ *DoF*).

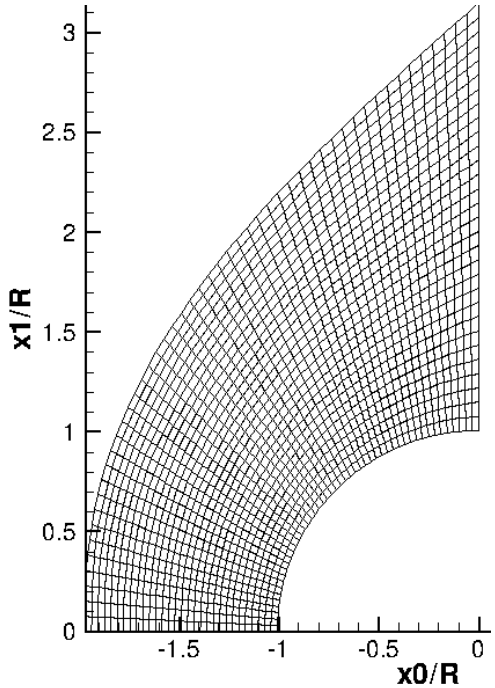

(b) Quadrilateral mesh, 30×100 nodes(3×10^3 *DoF*).

Figure 3: Meshes employed (only upper half shown).

values prevents the solution to converge, see Table 2.

Table 2: Carbuncle fix sensitivity to ϵ_s.

ϵ_s	Pe^{Ω_i}	Result
0.01	100.0	Carbuncle
0.05	20.0	Carbuncle
0.1	10.0	No carbuncle
0.5	2.0	Diverges
1.0	1.0	Diverges

The link between ϵ_s and the cell Péclet number established before helps to explain the optimality of the $\epsilon_s \sim 0.1$ value, since the corresponding $Pe^{\Omega_i} \sim 10.0$ offers the maximum dissipation while staying on the advection dominated regime, where *RD* schemes are known to perform better [22].

Fig. 4c shows the region where the carbuncle fix is active: the accurate location provided by the shock detector in Eq. 14 is evident.

The convergence history corresponding to the solution in Fig. 4b is shown in Fig. 4d. The CFL number is increased exponentially up to 64. At this point the solution looks already like the one shown in Fig. 4b, but the residual is still high. Therefore, the value of μ_s is *frozen* (not recomputed anymore), in the spirit of what it is done for the flux limiter values in *FV* methods, [23]. Immediately after the *freezing*, the solution converges to the solution we show in Fig. 4b.

Consider now computing the same $Ma_\infty = 15$ problem on a 31×201 nodes mesh. For the same tangential spacing, the computational cells are comparatively more elongated across the shock surface, meaning this coarser mesh is even more prone to induce a carbuncle

instability, as discussed in section 1. This is indeed the case, as the optimal value of $\epsilon_s = 0.1$ we found for the 30×400 mesh leads to an anomalous solution, Fig. 6a where even an asymmetric recirculation region can be visible, Fig. 6b. Increasing the dissipation ($\epsilon_s = 0.2$, $Pe^{\Omega_i} = 5$) results in an acceptable solution Fig. 6c proving therefore the effectiveness of the fix in removing shock instabilities. However, the solution obtained does not converge even when freezing the computation of μ_s, Fig. 6d; most probably because the shock thickening due to the excessive dissipation level prevents the numerical shock wave to find a steady location, inducing a limit cycle behavior. In section 4 we will present a strategy to increase the effectiveness of the carbuncle fix for relatively lower values of ϵ_s.

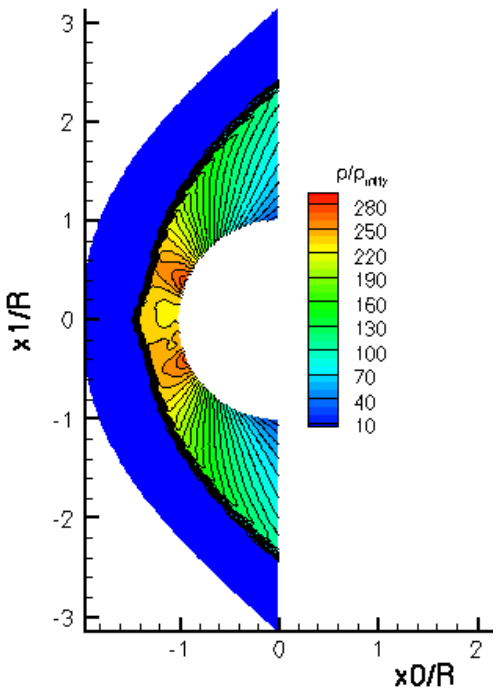

(a) p/p_∞ field - Standard fix, ϵ_s=0.05.

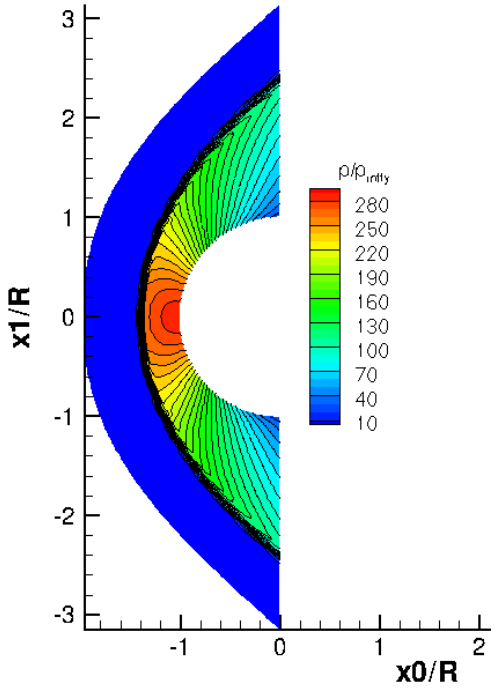

(b) p/p_∞ field - Standard fix, ϵ_s=0.1.

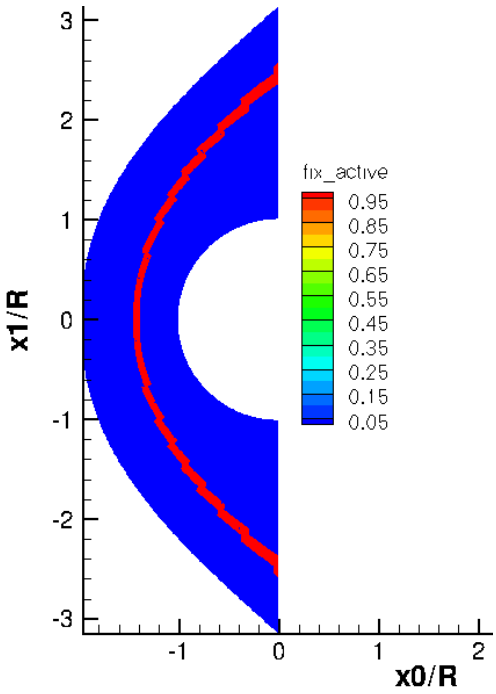

(c) Fix activation region for 4b.

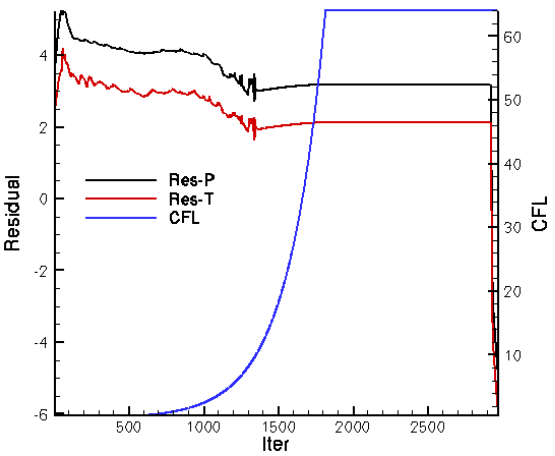

(d) Convergence history.

Figure 4: *RD* N scheme with Carbuncle Fix. $Ma_\infty = 15$ flow on 31×401 nodes mesh.

3.3. Results: FV and Carbuncle Fix

Results shown so far prove that a properly designed artificial diffusion term acting locally on the numerical shock wave can be effective as a remedy against carbuncle instabilities for *RD* methods. Nothing prevents, though, to discretize Eq. 9 with other numerical techniques. In this section we show how the carbuncle fix works correctly as well in the context of *FV* discretizations.

We consider a standard cell-centered *FV* solver, employing Roe scheme [26] with limited least-squares reconstruction at the inter-volume faces for the advective terms and a Green-Gauss strategy for the artificial diffusive term [27]. The steady solution to the discretized equations is obtained again through a pseudo-time stepping technique relying on a Krylov subspace method to solve for the resulting linear system. In particular, the *FV* solver employed to perform the simulations to follow is the one provided by the `COOLFluiD` computational framework [16].

We address again the testcase described in Table 1. Fig. 5 summarizes the results obtained. A 30×100 quadrilateral elements mesh (with 30 equispaced nodes over the cylinder wall and 100 nodes along the radial direction, see Fig. 3b) has been employed: we have been constrained to use such a coarse mesh to test our carbuncle fix, because the 30×400 and 30×200 meshes initially considered were not producing a distinct carbuncle as the one in Fig. 1b, but post-shock anomalies similar to those appearing in *RD* solutions when too low ϵ_s is used, Fig. 4a or 6a. This fact supports the claims that dimensionally-splitted *FV* methods introduce comparatively more numerical dissipation that multi-dimensional upwind techniques [28].

For the *FV* computations, the effectiveness of the shock fix is greatly affected by its activation region: having the fix active exclusively in the normal shock region (Eq. 13, Figures 5a and 5c) requires a higher dissipation level ($\epsilon_s = 0.1$) to prevent shock anomalies to appear than having it active throughout the whole numerical shock region (Eq. 14,

Figures 5b and 5d), where $\epsilon_s = 0.05$. On top of that, the abrupt change in μ_s at points $\frac{\vec{x}}{R} \approx (-1.2, \pm 0.9)$ hampers the convergence towards steady state: in fact, the computation with detector Eq. 13 blows up during the CFL increase phase: the flow field shown in Fig. 5a is actually the solution immediately before the computation diverges. Conversely, the convergence properties when using Eq. 14 as shock detector are favorable indeed: residuals decrease by ten orders of magnitude even before the CFL ramping procedure has finished, and no freezing of μ_s is necessary, see Fig. 5f.

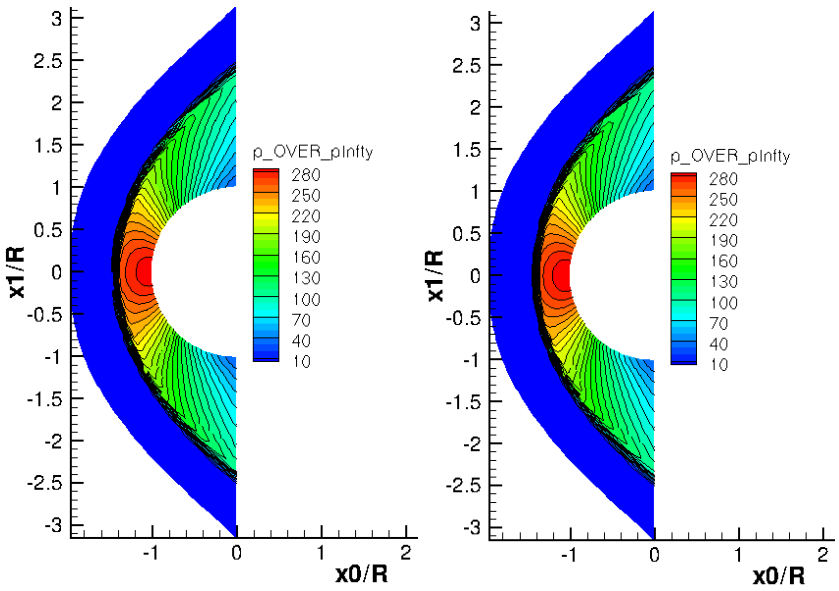

(a) p/p_∞ field - Detector Eq. 13, $\epsilon_s = 0.1$.

(b) p/p_∞ field - Detector Eq. 14, $\epsilon_s = 0.05$.

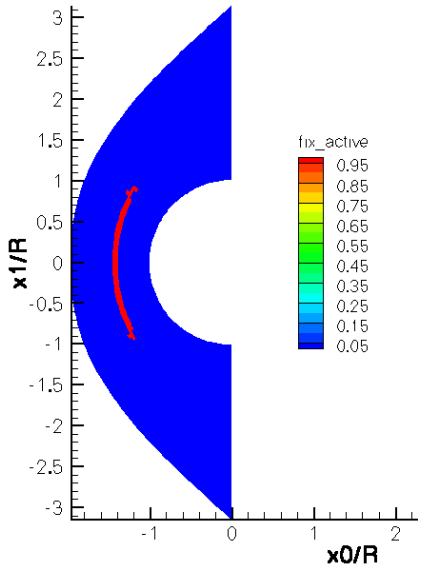

(c) Fix activation region for 5a.

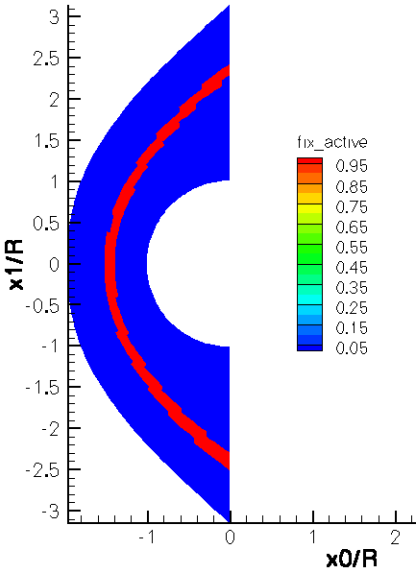

(d) Fix activation region for 5b.

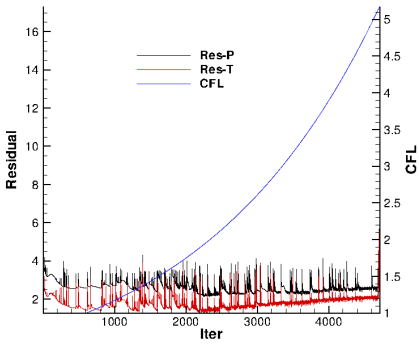

(e) Convergence history - Shock detector Eq. 13.

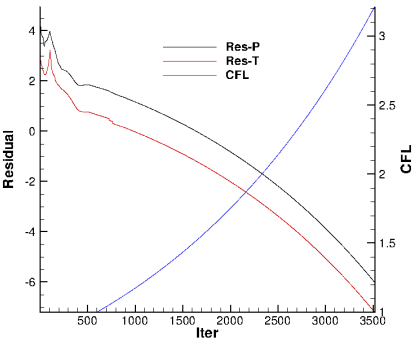

(f) Convergence history - Shock detector Eq. 14.

Figure 5: *FV Roe* scheme with Carbuncle Fix. $Ma_\infty = 15$ flow on 30×200 nodes mesh.

4. An energy-dissipative carbuncle fix

Attentive inspection of Eq. 9 reveals that the modification of the momentum equation introduced by the fix does not impact on the energy conservation equation. However, in a compressible flow, the elements in $\vec{U}$ are coupled through the equation of state, Eq. 4. This observation becomes clearer if we express Eq. 9 in the compact form we presented in section 2:

$$\frac{\partial \vec{U}}{\partial t} + \nabla \cdot \bar{\bar{F}}^c = \vec{\Delta}, \text{ with } \vec{\Delta} = \frac{\partial}{\partial \eta}\left(\mu_s \frac{\partial u_\xi}{\partial \eta}\right) \vec{1}_{\rho\, u_\xi}, \tag{18}$$

and compare it to the Navier-Stokes equations for a viscous flow:

$$\frac{\partial \vec{U}}{\partial t} + \nabla \cdot \bar{\bar{F}}^c = \nabla \cdot \bar{\bar{F}}^d. \tag{19}$$

We need therefore to express term $\vec{\Delta}$ in Eq. 18 in divergence form. For the sake of simplicity of exposition we present our reasoning for the `2D` case; extension to the `3D` case is straightforward.

Consider first the physical dissipative tensor $\bar{\bar{F}}^d$, in a Cartesian frame of reference for a `2D` flow by (see [14]):

$$\bar{\bar{F}}^d = \left(A_{xx}\frac{\partial \vec{P}}{\partial x} + A_{xy}\frac{\partial \vec{P}}{\partial y}\right) \vec{1}_x^t + \left(A_{yx}\frac{\partial \vec{P}}{\partial x} + A_{yy}\frac{\partial \vec{P}}{\partial y}\right) \vec{1}_y^t \tag{20}$$

where vector $\vec{P}$ is the vector of the primitive variable set:

$$\vec{P} = \left[\rho,\, \vec{v}^t,\, T\right]^t, \tag{21}$$

and the matrices $A_{x_i\, x_j}$ are 4×4 square matrices whose rows tell how the dissipative phenomena affect each of the conservation equations: 1^{st} row is for the mass conservation equation, 2^{nd} and 3^{rd} for the two components of the momentum conservation equation, and the last one for the total energy conservation equation. For Newtonian fluids, which present an isotropic behavior, $A_{yx} = A_{xy}^t$.

The structure of Eq. 20 is conserved if the diffusive tensor is expressed in any Cartesian, right handed system of reference. If we write now the carbuncle fix in its original form (Eq.18) as in Eq. 20, only $A_{\eta\,\eta}$ is non zero:

$$A^{Original}_{\eta\,\eta} = \begin{bmatrix} 0 & 0 & 0 & 0 \\ 0 & \mu_s & 0 & 0 \\ 0 & 0 & 0 & 0 \\ 0 & 0 & 0 & 0 \end{bmatrix} \tag{22}$$

Eq. 22 respects the consensus throughout the carbuncle bibliography of the connection between transverse perturbations, their variations along the shock surface and the shock instability. Let us compare Eq. 22 with matrix A_{yy} in Eq. 20 (once expressed in the (ξ, η) system of reference, and with the assumption $\mu_v = -\frac{2}{3}\mu$ for the bulk viscosity coefficient):

$$A^{Physical}_{\eta\,\eta} = \begin{bmatrix} 0 & 0 & 0 & 0 \\ 0 & \mu & 0 & 0 \\ 0 & 0 & \frac{4}{3}\mu & 0 \\ 0 & \mu\, u_\xi & \frac{4}{3}\mu\, u_\eta & \kappa \end{bmatrix}. \tag{23}$$

The main differences are the inclusion of transversal variations of u_η (that might be non-zero at the numerical level) and T, and the fact that the *dissipation* of momentum is accompanied by a **consistent** dissipation of energy. Notice also all the eigenvalues of $A_{\eta\,\eta}$ are either positive or zero (precisely, the definition of positive semi-definiteness), what is in line with the proper entropy dissipation advocated for in [11].

We can define a dissipative matrix with the same structure as in Eq. 23 (denoted from now on as $A^{ED}_{\eta\,\eta}$) to construct an Energy-Dissipative (or *ED*) carbuncle fix just by applying the associated diffusive tensor in the cells where either Eq. 13 or Eq. 14 (preferably) are not zero.

$$\bar{\bar{F}}^{ad} = A^{ED}_{\eta\,\eta} \frac{\partial \vec{P}}{\partial \eta}\, \vec{1}^t_\eta \tag{24}$$

At the sight of Eq. 23, we realize that we have gained full control of the way our artificial diffusion acts. For example we could choose to keep only the terms affecting variations

of u_ξ (the second column), obtaining a carbuncle fix with the consistent energy dissipation. Or we could decide to consider contributions from the variations of T to the energy conservation equation, since variations in energy affect the pressure field. Other alternative choices are possible and explorable. Thus, more than a single carbuncle fix, we have derived a complete family of them.

4.1. RD discretization of the ED carbuncle fix

Any member of the family of fixes described by Eq. 24 is discretized using Galerkin method, exactly as for Eq. 11. As an example, we present the discretization of the carbuncle fix obtained considering contributions from u_ξ and T variations:

$$\vec{\Phi}_l^{ad} = -\mu_s \frac{n_{\eta,l}}{2} \left.\frac{\partial u_\xi}{\partial \eta}\right|^h \left(\vec{1}_{\rho\, u_\xi} + \bar{u}_\xi, \vec{1}_{\rho\, E}\right) - \kappa_s \frac{n_{\eta,l}}{2} \left.\frac{\partial T}{\partial \eta}\right|^h \vec{1}_{\rho\, E} \tag{25}$$

where $\frac{\partial}{\partial \eta}|^h$ and $\bar{u}_\sigma$ stand, respectively, for the discretization of derivative $\frac{\partial m}{\partial \eta}$ for any magnitude m and for an average of u_σ ($\sigma = \xi, \eta$) over the cell where the fix is applied. They are given by:

$$\left.\frac{\partial m}{\partial \eta}\right|^h = \frac{1}{2\,\Omega_i} \sum_{k=1}^{3} n_{\eta,k}\, m_k, \quad \bar{u}_\sigma = \tfrac{1}{3} \sum_{k=1}^{3} u_{\sigma,k}. \tag{26}$$

The different vectors and nodal quantities needed are given by expressions similar to those in Eq.12.

In order not to increase the number of parameters controlling the fix performance, κ_s is related to μ_s considering a fixed Prandtl number of $Pr = 0.71$, as:

$$\kappa_s = \frac{\mu_s\, C_p}{Pr}. \tag{27}$$

where C_p is the specific heat capacity at constant pressure of the gas at hand, $C_p = C_v + R_g$, assuming a perfect gas behavior.

4.2. Results: RD and ED Carbuncle Fix

Consider once again the $Ma_\infty = 15$ problem on the previously considered 31×201 nodes triangular mesh, and recall that setting $\epsilon_s = 0.2$ was required by the Standard carbuncle fix in order to obtain the reasonably looking solution in Fig. 6c with the residuals stalling at a too high value, Fig. 6d.

Now, if the *ED* fix described by Eq. 25 is applied to the same problem, an artificial dissipation proportional to just $\epsilon_s = 0.1$ suffices to obtain the solution shown in Fig. 6e, with a convergence to steady state as in Fig. 6f (after freezing μ_s): more physically consistent diffusion terms employed as carbuncle fix allow to employ lower dissipation levels and interfere less with the convergence to steady state properties of the pseudo-time iterator.

Finally, and in order to assess the superior robustness of the *ED* fix, we consider a $Ma_\infty = 30$ problem: we compute *RD* solutions on a 31×401 nodes triangular mesh, using alternatively the standard (Eq. 11) and the *ED* (Eq. 25) fixes. The results obtained are summarized in Fig. 7. Again an $\epsilon_s = 0.1$ introduces enough dissipation to prevent the carbuncle formation for both fixes[3], Figures 7a and 7a. However, inspection of the Ma field reveals that the standard fix solution (Fig. 7c) presents overshoots (Ma>40 in a $Ma_\infty = 30$ problem!) across the numerical shock surface, meaning the positivity of system N scheme has been compromised. No overshoots appear for the solution computed with the *ED* fix, Fig. 7d. And to conclude, the convergence to steady state of the standard fix computation, Fig. 7e cannot be achieved while it presents no problem when the *ED* fix is used, Fig. 7f.

The benefits of employing a more physically consistent diffusive term are therefore evident, since lower levels of dissipation fulfill the objective of preventing the carbuncle

[3] And exemplifying once again the carbuncle is determined to a large extent by the computational grid employed.

growth while allowing better convergence to steady state.

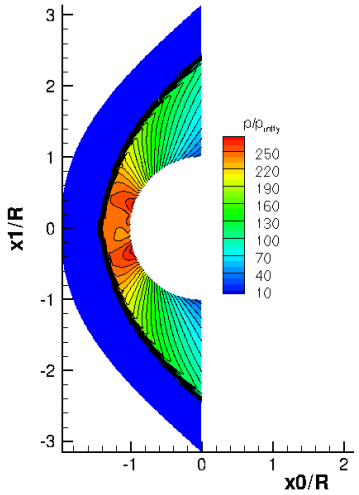

(a) p/p_∞ field - Standard fix, ϵ_s=0.1.

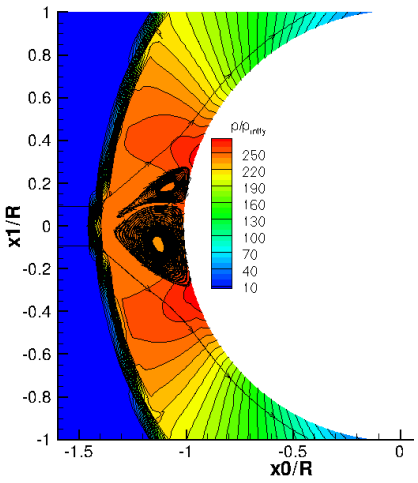

(b) Close-up near stagnation point for Fig. 6a.

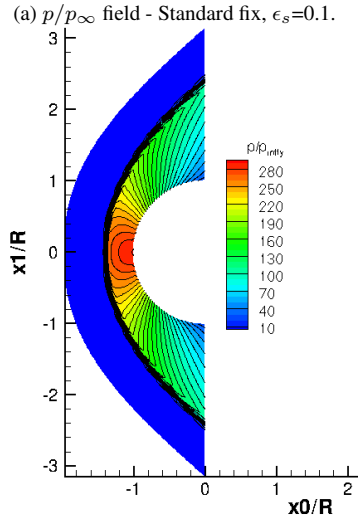

(c) p/p_∞ field - Standard fix, ϵ_s=0.2.

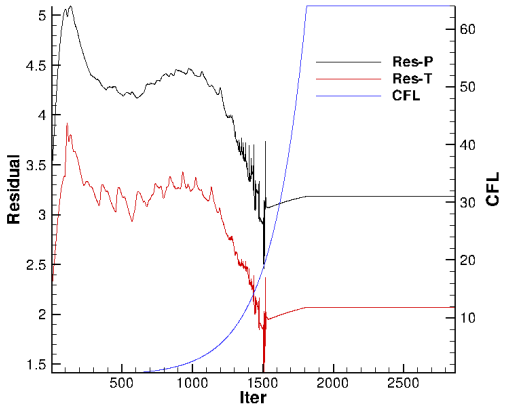

(d) Convergence history for Fig. 6c.

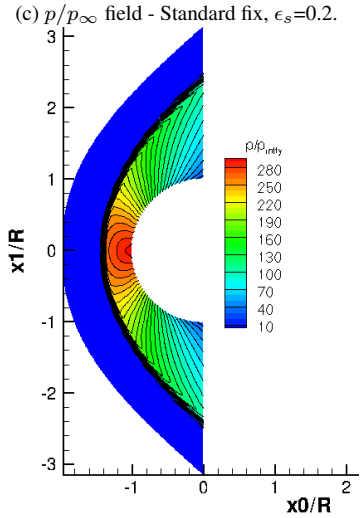

(e) p/p_∞ field - *ED* fix, ϵ_s=0.1.

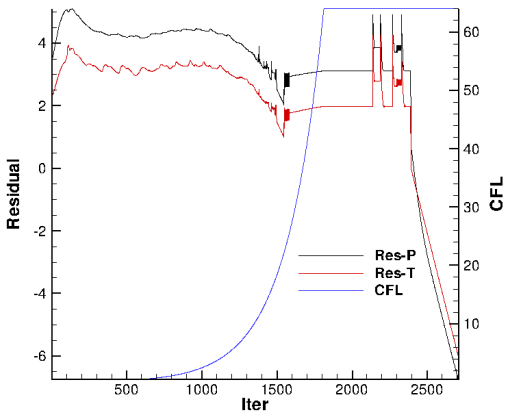

(f) Convergence history for Fig. 6e.

Figure 6: *RD* N scheme with Carbuncle Fix. $Ma_\infty = 15$ flow on 31×201 nodes mesh.

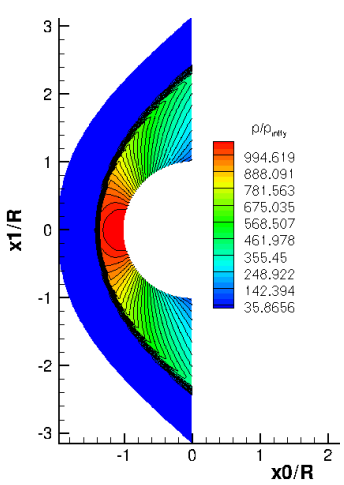

(a) p/p_∞ field - Standard fix, ϵ_s=0.1.

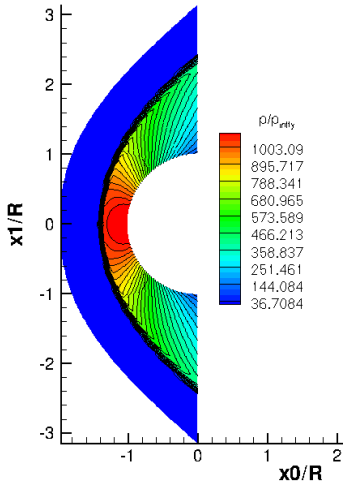

(b) p/p_∞ field - *ED* fix, $\epsilon_s = 0.1$.

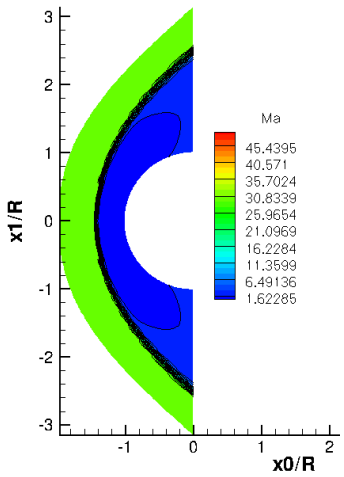

(c) Ma field - Standard fix, ϵ_s=0.1.

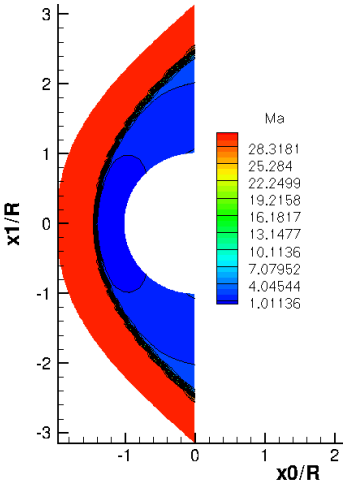

(d) Ma field - *ED* fix, $\epsilon_s = 0.1$.

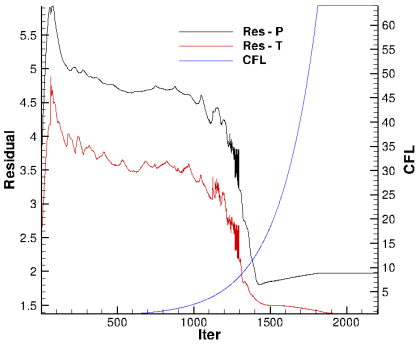

(e) Convergence history - Standard fix, ϵ_s=0.1.

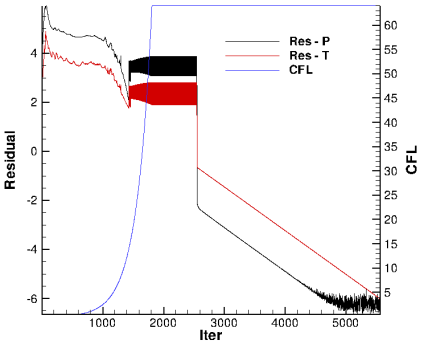

(f) Convergence history - *ED* fix, $\epsilon_s = 0.1$.

Figure 7: *RD* N scheme with Carbuncle Fix. $Ma = 30$ testcase on 30×200 nodes mesh.

5. Conclusions

The Residual Distribution carbuncle fix in Ref. [15]) has been thoroughly analyzed. The fix, which is formulated as a locally active artificial diffusive term, depends on a single controlling parameter ϵ_s. We have been capable to relate this parameter ϵ_s with a local Péclet-like number through an adequate redefinition of the artificial dissipation coefficient. This fact allows to justify why the fix performs optimally for $Pe \sim 10$, as this amounts to introducing a maximum of dissipation while staying in a convection-dominated regime.

The flexibility of the artificial diffusion-based fix is demonstrated by employing it, for what -we believe- the first time, in the context of a cell-centered *FV* discretization: carbuncle instabilities are equally avoided in this case. These *FV* results show the shock fix presented here is compatible with any discretization technique capable of handling dissipative terms.

Finally, the beneficial effect of more physically consistent (Energy-Dissipative, or *ED*) fixes has been proven: we linked the observation that the standard fix can lose its efficiency for certain poorly constructed meshes -after all, the carbuncle instability is a phenomenon largely dependent on the grid employed, as the extensive bibliography confirms- with the fact that the standard fix acts exclusively on the momentum equation; it turns out that supplementing the momentum dissipation with a consistent energy dissipation (mimicking that of a physical diffusive term) helps the fix to recover its effectiveness and good convergence properties.

AppendixA. Residual Distribution Solver - Details

A very short review of *RD* for the discretization of System of Eqs. 18 is presented in this appendix. The interested reader will find extensive explanations in references [8, 29, 22].

Given the physical domain Ω, and assuming a tesselation (n_{Elem} tetrahedra/triangles, n_{DoF} vertices) into linear simplicial ($P1$) elements Ω^h is available, the solution sought can be expressed in terms of the associated nodal Lagrangian basis function, as:

$$\vec{U}^h(\vec{x},t) = \sum_{j=1}^{n_{DoF}} \vec{U}_j(t)\, N_j(\vec{x})\,. \tag{A.1}$$

Basis functions N_l are piece-wise linear (more popularly, *tent-shaped*) and have compact support, that is, they differ from zero only in the close neighborhood of vertex l. We define Ξ_l precisely as:

$$\Xi_l \equiv \left\{\Omega_i \in \Omega^h \mid N_l(\vec{x}) \neq 0 \text{ if } \vec{x} \in \Omega_i\right\}. \tag{A.2}$$

Relation $N_l(\vec{x}_k) = \delta_{jk}$ holds as well, where δ_{lk} is the Kronecker tensor; ***RD*** schemes are therefore *vertex-centered* techniques. Finally, N_l functions are such that its gradient restricted to an element $\Omega_i \in \Xi_l$ is:

$$\left.\frac{\partial N_l}{\partial x_j}\right|_{\Omega_i} = \frac{1}{n_D \Omega_i} n_{l,j}, \tag{A.3}$$

where $\vec{n}_k$ is the scaled inward-pointing face normal, and Ω_i represents in this context the volume (or area) of the element. This property allows to express the discrete gradient $\nabla\vec{U}^h$ as:

$$\left.\frac{\partial \vec{U}^{\,h}}{\partial x_j}\right|_{\Omega_i} = \sum_{k\in\Omega_i} \vec{U}_k \frac{\partial N_k}{\partial x_j} = \sum_{k=1}^{n_D+1} \frac{1}{n_D \Omega_i} \vec{U}_k n_{j,k}. \tag{A.4}$$

The steady state residual for cell Ω_i is defined as:

$$\vec{\Phi}^{\Omega_i} = \int_{\Omega_i} \left(\frac{\partial \vec{F}_j^{\,c}}{\partial x_j} - \frac{\partial \vec{F}_j^{\,ad}}{\partial x_j}\right) dV = \vec{\Phi}^{c} - \vec{\Phi}^{ad}, \tag{A.5}$$

with contributions from the convective and the *artificial* dissipative terms.

A system of equations for the evolution in pseudo-time towards the steady state solution is obtained by collecting *fractions* of the cell residuals $\vec{\Phi}^{\Omega_i}$, that is, for node l such system is:

$$V_{\Xi_l} \frac{d\vec{U}_l}{dt} + \sum_{\Omega_i \in \Xi_l} \left(\mathfrak{f}^c\left(\vec{\Phi}^{c,\Omega_i}\right) + \mathfrak{f}^d\left(\vec{\Phi}^{ad,\Omega_i}\right)\right) = \vec{0}, \tag{A.6}$$

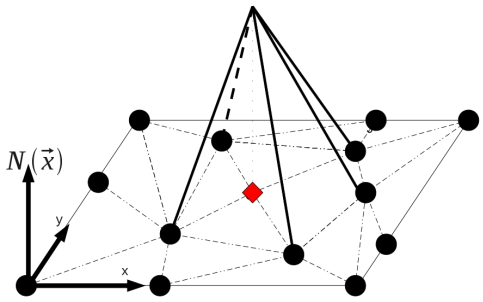

Figure A.8: $P1$ nodal basis function for l-th node.

where V_{Ξ_l} stands for the volume of the median dual cell around l-th node. The operation of *fractioning* or distributing the residual towards node l is represented by operators $\mathfrak{f}^c$ and $\mathfrak{f}^d$.

Different choices for $\mathfrak{f}^c$ define different schemes. In general, $\mathfrak{f}^c$ is given in terms of the so called nodal upwind parameters:

$$K_k = \frac{1}{n_D} A^{c,U}_{x_d}\, n_{x_d,k}, \text{ and } k \in \{1, \ldots, n_D + 1\}\,. \tag{A.7}$$

A_{j,x_d} is the Jacobian of the advective flux along direction x_d, and n_{j,x_d} are the components of the vectors normal to the element faces.

In this work we distribute the convective residuals with the N-scheme [8], given by:

$$\vec{\Phi}^{c,\Omega_i,N}_l = K^+_l \cdot \left(\vec{U}_l - \vec{U}^{\Omega_i}_{inlet}\right). \tag{A.8}$$

where the *inlet* state $\vec{U}^{\Omega_i}_{inlet}$ reads:

$$\vec{U}^{\Omega_i}_{inlet} = \left(\sum_{j\in\Omega_i} K^-_j\right)^{-1} \cdot \sum_{j\in\Omega_i} K^-_j \cdot \vec{U}_j. \tag{A.9}$$

The N scheme is linear, multid-dimensional upwind and *positive*; hence it is only 1^{st} order accurate.

Distribution of diffusive contributions to the cell residual is done, when a $P1$ element mesh is used, by Galerkin discretization:

$$\vec{\Phi}^{d,U}_l = \int_\Omega N_l\, \nabla \cdot \bar{\bar{F}}^v\, dV. \tag{A.10}$$

Acknowledging the basis functions N_l have compact support, we are left with:

$$\vec{\Phi}_l^d = \int_\Omega N_l \frac{\partial \vec{F}_j^v}{\partial x_j}\, dv = \int_{\Xi_l} N_l \frac{\partial \vec{F}_j^v}{\partial x_j}\, dv = \sum_{\Omega_i \in \Xi_l} \int_{\Omega_i} N_l \frac{\partial \vec{F}_j^v}{\partial x_j}\, dv. \tag{A.11}$$

Integration by parts and application of Gauss theorem transform previous equation into:

$$\vec{\Phi}_l^d = \oint_{\Xi_l \cap \delta\Omega} N_l \vec{F}_j^v 1_j^{ext} ds - \sum_{\Omega_i \in \Xi_l} \int_{\Omega_i} \frac{\partial N_l}{\partial x_j} \vec{F}_j^v dv. \tag{A.12}$$

First term on the *RHS* of last equation is relevant only for elements lying on the external boundary, $\delta\Omega \cap \Xi_l \neq \emptyset$, Ref. [8]. Second term on the *RHS* collects the diffusive contributions to the nodal residual. Its discrete form, by using Eqs. A.3 and A.4, is:

$$\vec{\Phi}_l^d = -\sum_{\Omega_i \in \Xi_l} \frac{1}{2} n_{j,l} \vec{F}_j^v \left(\mu_{avg}, \lambda_{avg}, \vec{U}_{avg}, \nabla \vec{U}^h\right). \tag{A.13}$$

Acknowledgments

First author has been supported by a Belgian *FRIA* fellowship from the *Fonds National de la Recherche Scientifique*.

References

[1] J. Quirk, A contribution to the great riemann solver debate, International Journal for Numerical Methods in Fluids 18 (6) (1994) 555–574.

[2] R. Sanders, E. Morano, M.-C. Druguet, Multidimensional dissipation for upwind schemes: stability and applications to gas dynamics, Journal of Computational Physics 145 (1998) 511–537.

[3] J.-C. Robinet, G. J., G. Casalis, J.-M. Moschetta, Shock wave instability and carbuncle phenomenon: same intrinsic origin?, Journal of Fluid Mechanics 417 (2000) 237–263.

[4] M. Pandolfi, D. D'Ambrosio, Numerical instabilities in upwind methods: analysis and cures for the carbunclephenomenon, Journal of Computational Physics 166 (2) (2001) 217–301.

[5] M. Dumbser, J.-M. Moschetta, J. Gressier, A matrix stability analysis of the carbuncle phenomenon, Journal of Computational Physics 197 (2) (2004) 647–670.

[6] S. J. Henderson, Study of the issues of computational aerothermodynamics using a riemann solver, Ph.D. thesis, Wright State University (2007).

[7] K. Kitamura, E. Shima, Y. Nakamura, P. Roe, Evaluation of euler fluxes for hypersonic flow computations, AIAA Journal 48 (4) (2010) 763–776.

[8] E. van der Weide, Compressible flow simulation on unstructured grids using multi-dimensiona upwind schemes, Ph.D. thesis, Technische Universitet Delft (1998).

[9] B. Einfeldt, On godunov-type methods for gas dynamics, SIAM Journal on Numerical Analysis 25 (2) (1988) pp. 294–318.

[10] A. Harten, High resolution schemes for hyperbolic conservation laws, Journal of Computational Physics 135 (2) (1994) 555–574.

[11] F. Ismail, Towards a reliable prediction of shocks in hypersonic flow: resolving carbuncles with entropy and vorticity control, Ph.D. thesis, University of Michigan (2006).

[12] J. Anderson, Hypersonic and high temperature gas dynamics, $2^{nd}Ed$, AIAA Textbooks Series, American Institute of Aeronautics and Astronautics, 2006.

[13] A. Chorin, M. J.E., A Mathematical Introduction to Fluid Mechanics, 3^{rd} edition, Springer, 2000.

[14] C. Hirsch, Numerical Computation of Internal and External Flows: Introduction to the Fundamentals of CFD, 2^{nd} Edition, Butterworth-Heinemann, 2006.

[15] K. Sermeus, H. Deconinck, Solution of steady euler and navier-stokes equations using residual distribution schemes, LS 2003-05, VKI (2003).

[16] A. Lani, N. Villedieu, K. Bensassi, L. Kapa, M. Vymazal, M. S. Yalim, M. Panesi, COOLFluiD: an open computational platform for multi-physics simulation and research, in: AIAA 2013-2589, 21th AIAA CFD Conference, San Diego (CA), 2013.

[17] P. A. Gnoffo, Updates to multi-dimensional flux reconstruction for hypersonic simulations on tetrahedral grids, in: Proceedings of the 48^{th} AIAA Aerospace Science Meeting and Exhibit, AIAA, Orlando(FL), 2010.

[18] Garicano Mena, J. and Lani, A. and Sermeus, K. and K. and Deconinck, H., An effective treatment of numerical shock wave instabilities with residual distribution schemes: Application to hypersonic nonequilibrium flows around blunt bodies, in: 7^{th} European Symposium on Aerothermodynamics for Space Vehicles, Brugge, Belgium, 2011.

[19] R. Prabhu, An implementation of a chemical and thermal nonequilibrium flow solver on unstructured meshes and applications to blunt bodies, CR 194967, NASA (1994).

[20] Y. Saad, Iterative methods for sparse linear systems: Second edition, SIAM, 2003.

[21] S. Balay, J. Brown, K. Buschelman, V. Eijkhout, W. D. Gropp, D. Kaushik, M. G. Knepley, L. C. McInnes, B. F. Smith, H. Zhang, Petsc users manual, Tech. Rep. ANL-95/11 - Revision 3.4, Argonne National Laboratory (2013).

[22] N. Villedieu, High order discretisation by residual distribution schemes, Ph.D. thesis, Université Libre de Bruxelles (2009).

[23] A. Lani, An object oriented and high-performance platform for aerothermodynamic simulations, Ph.D. thesis, Université Libre de Bruxelles (2008).

[24] K. Sermeus, Multi-dimensional upwind discretization and application to compressible flows, Ph.D. thesis, Université Libre de Bruxelles (2013).

[25] H. Deconinck, P. Roe, R. Struijs, A multidimensional generalization of Roe's flux difference splitter for the Euler equations, Computers and Fluids 22 (2-3) (1993) 215–222.

[26] P. Roe, Approximate Riemann Solvers, Parameter Vectors, and Difference Schemes, Journal of Computational Physics 43 (1981) 357–372.

[27] S. E. Kim, B. Makarov, D. Caraeni, Multi-dimensional linear reconstruction scheme for arbitrary unstructured mesh, in: AIAA-2003-3990, 16th AIAA CFD Conference, Orlando, Florida, 2003.

[28] H. Deconinck, K. Sermeus, R. Abgrall, Status of multidimensional upwind residual distribution schemes and applications in aeronautics, in: Proceedings of the AIAA Fluids 2000 Conference, Denver, 2000, AIAA, 2000.

[29] M. Ricchiuto, Construction and analysis of compact residual distribution discretizations for conservation laws on unstructured meshes, Ph.D. thesis, Université Libre de Bruxelles (2005).